COMPUTER SIMULATION OF FLOW-DEPENDENT
ABSORPTION IN MICROPERFUSED
SHORT HENLE'S LOOP OF RATS

A. D. BAINES, *Department of Clinical Biochemistry, University of Toronto,*
Toronto, Ontario M5G 1L5

D. BASMADJIAN AND B. C. WANG, *Department of Chemical Engineering and*
Applied Chemistry, University of Toronto, Toronto, Ontario M5S 1A4
Canada

ABSTRACT   With computer simulation we examined the extent to which current theories and experimental data explain function of single microperfused superficial Henle's loops in rats. In the model standard phenomenological equations describe transport; two sets of transport parameters labeled rat and rabbit were taken from published experiments; Michaelis-Menten kinetics in the ascending thick limb were adjusted arbitrarily; tubular radius is either constant or depends on luminal pressure with compliance based on experimental observations; the interstitium is an infinite sink with salt and urea concentrations constant in the cortex and exponentially increasing in the outer medulla; concentrations resemble those found in hydropenic or saline diuretic rats. The following predictions were obtained. The model with rabbit parameters does not recirculate urea and will not operate with high medullary urea concentrations; with rat parameters too much urea recirculates and the results of perfusion with equilibrium solution are not reproduced. Using a compromise between rat and rabbit parameters, the model reproduces water absorption, salt reabsorption, and urea recirculation as observed in vivo in rat loops perfused at 5–40 nl/min. It also simulates perfusion with saline, equilibrium solution, saline plus furosemide, and 300 mM mannitol. When the model includes a short early distal segment, effluent salt concentration reaches a minimum at a 15 nl/min perfusion rate as observed in vivo; however, concentration at the macula densa is a monotonically increasing function of flow. When permeation rate is a function of wall surface area and thickness a better fit to experimental results is produced. However, the effect is small: water absorption alters by 4% or less and effluent salt concentration is reduced by up to 10% at low perfusion rates. Comparison of rigid and compliant loops shows no relationship between transit time per se and reabsorption.

INTRODUCTION

Our understanding of Henle's loop function is limited because this complex structure lies almost completely within the kidney. Fluid entering and leaving short loops can be sampled on the cortical surface and the tips of long justamedullary loops are accessible on the papillary surface. However, functional relationships observed in the hairpin bend of long papillary loops may not apply to short loops that bend in the outer medulla. Function of long loops has been extensively modeled (18), but less has been done specifically about short loops. In the following paper we describe computer simulation of flow-dependent absorption in short superficial loops of rats.

In vivo microperfusion of superficial short loops with a variety of solutions shows that reabsorption is load-dependent in a nonlinear fashion (25, 32–35). Factors that could contribute to this load dependency are: unsaturated active transport systems, transmural osmotic pressure gradients, transmural hydrostatic pressure gradients, flow velocity, wall thickness, and wall surface area. The relative importance of these factors depends upon transport parameters of the wall.

Estimates for transport parameters in the pars recta (PR), long papillary descending thin limb (DTL), and ascending thick limb (ATL) are available from in vitro examinations of isolated rat papillae and isolated perfused fragments of rabbit tubules. Transport parameters of rat tubules measured in isolated papillae are not the same as those of rabbit tubules measured in isolated perfused fragments (18). However, when the technique of isolated tubule perfusion was used to examine both rat and rabbit thin ascending limbs, it appeared that transport parameters were similar in the two species (16). Unfortunately, no measurements have been made on the DTL of short superficial loops, therefore for our mathematical simulation we were forced to choose from the estimates of transport parameters in the long DTL. We began by selecting two possible extreme types of DTL from experimental data. The final model incorporates a compromise set of data resembling rat more than rabbit parameters.

Transit time and luminal diameter often appear as potentially significant factors influencing loop function (1, 5, 7, 32). These factors could only be examined by making the model loop distensible. Using equations that describe the compliance of isolated perfused tubules (40), we attempted to simulate the experimentally observed relationships between flows and pressures in the loop (23, 32). The compliant tubule model enabled us to examine the effect that radius-dependent permeabilities may have on loop function, and to compare the results with those obtained from rigid tubules with constant permeabilities.

The predictions of models incorporating various parameters were compared with data obtained from in vivo microperfusion experiments on rat superficial Henle's loops.

THE MODEL

Components of the model are described in the following order: equations governing water and solute transport across tubule walls and axially through the lumen; tubule dimensions, compliance and transit time; parameters describing wall permeability; active transport; composition of the interstitial compartment.

Transmural Flux Equations

The need to write equations that produce mass balance was avoided by making the reasonable assumption that the interstitium around a single microperfused loop acts as an infinite sink or source for water and solute. In a previous paper (6) we demonstrated theoretically that liquid resistance to radial transport in Henle's loop is insignificant even when concentration at the wall changes along the tubule and noncylindrical lumen shapes are assumed. As will be shown, axial diffusion does not appear to influence the results significantly. Therefore, movements of solute and water between lumen and peritubular space are determined solely by wall parameters, hydrostatic pressures, and the transmural concentration difference.

In the final model, wall parameters were either kept constant (rigid tubule) or modified to account for changes in wall thickness and surface area in a compliant tubule. To incorporate this dependence, the volume of cells in the wall was assumed constant; therefore, wall thickness was inversely proportional to luminal radius, and permeability varied directly with radius.

Equations describing the transmural fluxes of solutes and water were adapted from linear nonequilibrium thermodynamic theory (9). For water transport:

$$J_v = L_p R_g T \Sigma \left(\sigma_i \Delta C_i \right) - L_f P, \tag{1}$$

where R_g is the gas constant ($82.06 \text{ atm} \cdot \text{cm}^3 \cdot \text{mol}^{-1} \cdot {}^\circ \text{K}^{-1}$), T is temperature (°K), P is transmural pressure (atmospheres), J_v is water flux ($\text{cm}^3 \cdot \text{s}^{-1} \cdot \text{cm}^{-2}$), L_p is osmotic permeability of the wall, L_f is hydraulic permeability ($\text{cm}^3 \cdot \text{cm}^{-2} \cdot \text{s}^{-1} \cdot \text{atm}^{-1}$), σ_i is the reflection coefficient for the i-th solute, and ΔC_i is the concentration difference of the i-th solute across the wall. In this paper $L_p = L_f$.

For solute transport:

$$J_i = K_i \left(\Delta C_i \right) + J_v \left(1 - \sigma_i \right) \overline{C}_i + A_i / 2\pi R, \tag{2}$$

where J_i is the dissipative solute flux across the wall ($\text{mol} \cdot \text{s}^{-1} \cdot \text{cm}^{-1}$), K_i is the permeability coefficient of the i-th solute across the wall, $\overline{C}_i$ is the mean of the i-th solute concentration on either side of the wall, A_i is an active transport term ($\text{mol} \cdot \text{cm}^{-1} \cdot \text{s}^{-1}$), and R is radius (centimeters).

Transport Equations

The conventional rate equations for passive transmural flow of solutes of water applied over a differential segment in the axial direction can be written in the two equivalent forms:

$$K' 2\pi R \, dx \cdot \Delta C = \frac{D}{h} 2\pi R \, dx \cdot \Delta C \tag{3}$$

K' is a transport coefficient; D is an equivalent effective diffusivity; h is wall thickness; and ΔC is the transmural concentration difference or driving force.

This formulation is strictly valid only for an infinitesimally thin wall. For a thick-walled tubule, corrections must be made for changes in wall area in the radial direction. These corrections are well known in the analogous case of heat conduction (e.g., Kreith [24], p. 30) and are easily translated into mass diffusion terms:

$$D \frac{2\pi}{R_e - R_i} \frac{R_e - R_i}{\ln \left[R_e / R_i \right]} \, dx \, \Delta C = K' 2\pi \frac{R_e - R_i}{\ln \left[R_e / R_i \right]} \, dx \cdot \Delta C_i, \tag{4}$$

where R_i and R_e are internal and external radii. The term $[R_e - R_i] / \ln [R_e / R_i]$ is known as the "log mean radius" ($\overline{R}$) and has a value between the two extremes of R_e and R_i.

To relate external to internal radius and calculate wall thickness, the constant wall volume condition is introduced:

$$[R_e^2 - R_i^2] = [R_e^2 - R_i^2]_r, \tag{5}$$

where $(R_e^2 - R_i^2)_r$ represents a set of reference radii and $(R_e - R_i)_r = h_r$, the wall thickness at the reference condition. Combining Eqs. 4 and 5, the following equivalent expressions for transmural transport are produced:

$$\frac{D}{h_r} \cdot \frac{2\pi(R_e - R_i)}{\ln(R_e/R_i)} \frac{(R_e - R_i)_r}{(R_e - R_i)} dx \, \Delta C = K \, 2\pi\overline{R}(h_r/h) \, dx \cdot \Delta C, \qquad (6)$$

where K is the transport coefficient at the reference conditions, and the dependence on R_e and R_i is abbreviated as $\overline{R}$ (h_r/h). Wall thickness, h, decreases as radius increases therefore, permeation rate increases not only because of the increased surface area but also because of a reduction in h. Thus the permeation varies with the square of the radius.

With these corrections for radius in hand, one can now combine differential water balance with Eq. 1 to obtain

$$\frac{dQ}{dx} = 2\pi\overline{R} \, (h_r/h) \, L_p \, (\sigma_s \Delta C_s + \sigma_u \Delta C_u) \, R_g T - 2\pi\overline{R} \, (h_r/h) \, L_f P, \qquad (7)$$

where Q is flow rate ($cm^3 \cdot s^{-1}$), subscripts s and u refer to salt and urea, respectively.

Eqs. 1 and 2 are similarly incorporated in differential solute and water balances to obtain Eqs. 8 and 9:

$$\frac{dC_s}{dx} = -\frac{1}{Q}\left[2\pi\overline{R}(h_r/h)K_s \, \Delta C_s - \frac{dQ}{dx}(1 - \sigma_s) \, \overline{C}_s + A_s + C_s \frac{dQ}{dx}\right], \qquad (8)$$

$$\frac{dC_u}{dx} = -\frac{1}{Q}\left[2\pi\overline{R}(h_r/h)K_u \, \Delta C_u - \frac{dQ}{dx}(1 - \sigma_u) \, \overline{C}_u + C_u \frac{dQ}{dx}\right]. \qquad (9)$$

Pressure-flow relationships are described by Poiseuille's equation:

$$\frac{dP}{dx} = -8\mu \, Q/\pi \, R_i^4 = -1.33 \times 10^{-5} \frac{Q}{R_i^4}, \qquad (10)$$

where μ is viscosity (poise). The validity of this relation for various tubule geometries is discussed in the companion paper (6).

Tubule Dimensions and Compliance, Transit Time

The initial model had three sections: the PR with a length of 0.5 cm; the DTL with a length of 0.15 cm; and the ATL with a length of 0.65 cm. These lengths were derived from the rat anatomical studies of Munkácsi and Palkovits (26). Shorter tubules would not reproduce observed transit times as well. The overall length is 1.3 cm; the tubule makes a 180° turn 0.65 cm from the origin (Fig. 1).

Tubular compliance measurements were obtained from recent experiments of Welling and Welling (40). Equations relating external radius (R_e) and transmural pressure (P) were fitted to the data for intact tubule segments given in Fig. 1 of reference (40) (Table I). R_i was calculated from Eq. 5. Early distal tubules are assigned the same compliance as ATL. Relationships between R_i and luminal pressure calculated in this way agree closely with those found for rat superficial proximal and distal tubules in vivo (8).

We assume that peritubular tissue pressure is constant and equal to atmospheric pressure
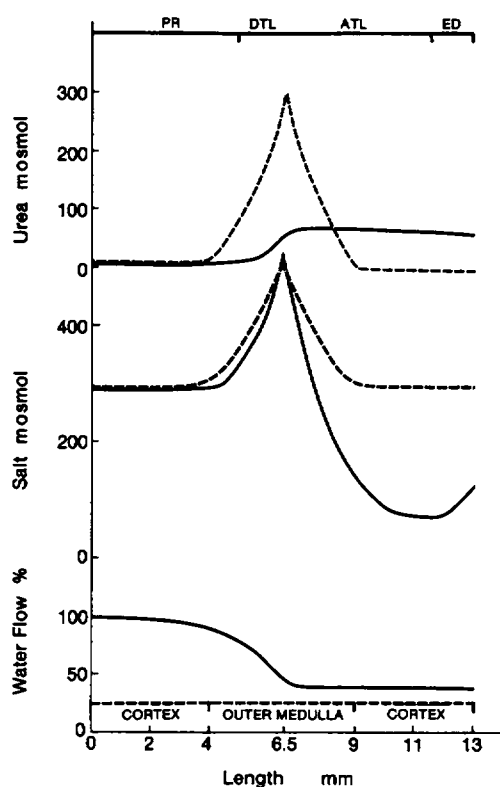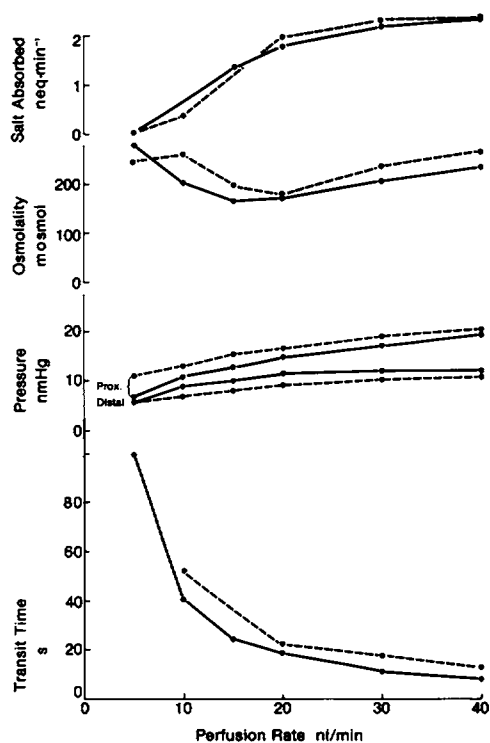
FIGURE 1

FIGURE 2

FIGURE 1 Solute concentrations along the model of Henle's loop with compromise parameters. Interstitial concentrations are shown as hatched lines and luminal concentrations as solid lines. Note that luminal salt concentration exceeds interstitial salt concentration at the midpoint of the loop. Perfusion rate (Q^0) is 10 nl/min. Percent water remaining in the lumen is shown at the bottom of the figure.

FIGURE 2 A comparison of data obtained from in vivo microperfusion of rat superficial Henle's loop (dashed line) and computer-simulated data using the compliant model with compromise parameters (solid line). Data for transit time and tubule pressures come from Schnermann (32); osmolality and salt absorption corrected for isotonic absorption come from Morgan and Berliner (25).

TABLE I
COMPLIANCES* AND REFERENCE RADII

Compliance	Reference radii
PR	$R_e = (15.9 + 0.63 \text{ P}\ddagger - 0.030 \text{ P}^2 + 0.0005 \text{ P}^3) \, 10^{-4} \text{ cm}$ $(R_e - R_i)_r = (20 - 11) \, 10^{-4} \text{ cm}$
DTL	$R_e = (9.6 + 0.49 \text{ P} - 0.023 \text{ P}^2 + 0.0004 \text{ P}^3) \, 10^{-4} \text{ cm}$ $(R_e - R_i)_r = (12.5 - 9.5) \, 10^{-4} \text{ cm}$
ATL	$Re = (11.3 + 0.65 \text{ P} - 0.033 \text{ P}^2 + 0.0005 \text{ P}^3) \, 10^{-4} \text{ cm}$
ED	$(R_e - R_i)_r = (15.6 - 10.0) \, 10^{-4} \text{ cm}$

*From reference 40.
‡P is measured in millimeters of Hg.

along the entire length of a single microperfused loop. Thus, transmural pressure used in compliance and transport equations is the same as luminal pressure used in Poiseuille's equation. The following summary indicates the magnitude of distortion introduced by this assumption.

Subcapsular fluid pressure in hydropenic rats is 1–2 mm Hg (20). Total tissue pressure has not been measured in rats but, in hydropenic dogs, tissue pressure measured with a diaphragm strain gauge (14) is similar to interstitial fluid pressure measured in implanted capsules (21). It is probable that outer cortical interstitial fluid and total tissue pressure are similar in hydropenic rats as they are in dogs.

Medullary tissue pressure is not likely to be greater than the pressure in collapsible structures such as veins and distal tubules, otherwise the lumens would be occluded. Interlobular vein pressure in the rat is 5 mm Hg (20). Furthermore, pressures in papillary and cortical capillaries are similar (29). Basing their argument on pressures in cortical and papillary tubules, Sanjana et al. (29) concluded that pressures in cortical and juxtamedullary distal tubules are similar. In hydropenic rats distal tubule pressure can be as low as 4 mm Hg (23). Thus, at most, medullary tissue pressure in hydropenic rats could be 2–4 mm Hg higher than subcapsular tissue pressure.

To calculate transit time, local variations in both flow rate and lumen radius are taken into account as follows:

$$d_t = \frac{\pi R_i^2}{Q} dx \text{ or } t = \int_0^L \frac{\pi R_i^2}{Q} dx. \tag{11}$$

Wall parameters

Table II gives the parameters we used initially to describe tubular wall characteristics. One group obtained partly from *in situ* measurements on rat kidneys is labeled rat. The other obtained from isolated rabbit tubules is labeled rabbit. Recent work (16) suggests that rabbit and rat parameters may not diverge as much as the values in Table II indicate.

For the sake of simplicity, Na^+ and its accompanying anions are treated as a single entity (salt) with a concentration equal to twice that of Na^+. Permeabilities and reflection coefficients for salt are assumed to be the same as for sodium. L_p was assumed to equal L_f.

Active salt transport

We have simplified active transport in the PR by combining sodium transport and bicarbonate transport into one term called salt transport. In isolated perfused segments of rabbit PR, sodium is transported at ≈ 1 neq cm^{-2} s^{-1}, whereas bicarbonate transport is estimated to be 0.3–0.8 neq cm^{-2} per s (31). We experimented with salt transport rates of 1–5 nosmol cm^{-2} s^{-1}; however, in all subsequent examples the rate was constant at 2 nosmol cm^{-2} s^{-1}. In the runs reported here active transport (A_s) was constant per unit length. The data in Table II are therefore expressed as osmol/cm per s.

When describing transport (A_s) in the ATL we used Michaelis-Menten kinetics as others have done (38). Morgan and Berliner (25) estimated total ATL salt transport by assuming that no water was reabsorbed in the ATL and that all salt reabsorbed in other segments was transported as an isotonic solution. It follows from these assumptions that salt transport in the ATL can be determined from total salt transport by the loop corrected for isotonic salt

TABLE II
TUBULE PARAMETERS

	Rat	Rabbit	Compromise
PR			
L_p, $10^{-5}\,cm^3\,cm^{-2}\,s^{-1}\,atm^{-1}$	18	3	7
K salt, $10^5\,cm\,s^{-1}$	9.3	9.3	2.1
σ salt	0.68	0.68	0.90
K urea, $10^{-5}\,cm\,s^{-1}$	11	5.3	3.7
σ urea	0.79	0.91	0.91
Active salt transport, $10^{-12}\,osM\,cm^{-1}\,s^{-1}$	15	15	15
DTL			
L_p, $10^{-5}\,cm^3\,s^{-2}\,atm^{-1}$	3.9	17	3.5
K salt, $10^{-5}\,cm\,s^{-1}$	47	1.6	28
σ salt	0.5	0.95	0.5
K urea, $10^{-5}\,cm\,s^{-1}$	13	1.5	7
σ urea	0.5	0.96	0.5
ATL			
L_p, $10^{-5}\,cm^3\,cm^{-2}\,s^{-1}\,atm^{-1}$	0.1	0.1	0.03
K salt, $10^{-5}\,cm\,s^{-1}$	6.3	6.3	4.4
σ salt	0.98	0.98	0.98
K urea, $10^{-5}\,cm\,s^{-1}$	1	1	0.7
σ urea	0.98	0.98	0.98
K_m, $mosmol\,kg^{-1}$	300	350	240
V_{max}, $10^{-12}\,osM\,cm^{-1}\,s^{-1}$	250	250	315
ED			
L_p, $10^{-5}\,cm^3\,cm^{-2}\,s^{-1}\,atm^{-1}$	0.1	0.1	0.03
K salt, $10^{-5}\,cm\,s^{-1}$	6.3	6.3	3.5
σ salt	0.98	0.98	0.5
K urea, $10^{-5}\,cm\,s^{-1}$	1	1	0.7
σ urea	0.98	0.98	0.7
K_m, $mosmol\,kg^{-1}$	300	350	100
V_{max}, $10^{-12}\,osM\,cm^{-1}\,s^{-1}$	250	250	13

Parameters for rat and rabbit from Table 7.1 in reference 18. Parameters for compromise PR from reference 31.

absorption. They found that salt transport calculated for the ATL in this way plateaued at the equivalent of 2.4 nosmol/min (25).

In the model, values for V_{max} and K_m were adjusted to satisfy three conditions: first, that salt absorption corrected for isotonic absorption should be 2.4 nosmol/min at a simulated perfusion rate of 40 nl/min (25); second, that salt concentration in the loop output should be 145 mosmol at a simulated perfusion rate of 20 nl/min (25); and third, that these conditions would be met when the perfusion solution was 295 mosmol salt and 5 mosmol urea. Once these three conditions were fulfilled, V_{max} and K_m were used unaltered in subsequent runs at different perfusion rates and with different perfusates.

External Solute Concentration

The interstitium is treated as an infinite sink. In the model, the cortical interstitium (Fig. 1) surrounds the proximal 4 mm of PR and the terminal 4 mm of the loop. Here the interstitial concentrations of salt and urea are designated constant at 295 mosmol and 5 mosmol, respectively. The outer medulla is 2.5 mm across and surrounds the distal 1 mm of PR and the

entire 1.5 mm of DTL. The loop then turns 180° so that the proximal 2.5 mm of ATL is also located in the outer medulla. Here interstitial solute concentration increases exponentially along the course of the PR and DTL and decreases exponentially along the course of the ATL.

In preliminary studies with rat and rabbit models the maximum external urea and salt concentration at the tip of the loop was adjusted to produce 45% water absorption from a saline solution perfused at 20 nl/min.

In the final model using compromise parameters, external salt and urea concentrations were set to resemble those observed in tissue slices from hydropenic or saline diuretic rats (4, 36) (Fig. 1). Maximum concentrations in the simulated hydropenic state were 500 mosmol salt and 300 mosmol urea. To simulate the saline diuretic state the concentrations were set at 500 mosmol salt and 50 mosmol urea (4).

When modeling the peritubular environment, we assumed that microperfusion of a single loop does not alter solute concentration about that loop. Our reasons for making this assumption are as follows. Taking, for an extreme example, that water is absorbed only in the DTL, then as perfusion goes from 5 to 40 nl/min radial water velocity increases from 6 to 18 $\times$ 10^{-5} cm/s. We have shown (6) that resistance to radial flux resides almost exclusively in the tubule wall and that these fluid velocities and the accompanying solute fluxes do not produce radial concentration gradients in the lumen. The same argument applies to radial solute concentrations in a narrow fluid compartment about the tubule.

Numerical Solution of Model

The complete model is comprised of the algebraic compliance relations given in Table I (omitted in the case of a rigid tubule), and the following four first order differential equations: solute and water balances (Eqs. 7, 8, and 9) and Poiseuille's law (Eq. 10). The required initial values are specified by conditions of the in vivo experiment being simulated: flow rate (Q^0) and composition (C_s^0, C_u^0) of fluid entering PR, and transmural pressure P^0 at the inlet.

The system was solved on an IBM 370/165 computer (IBM Corp., White Plains, N.Y.) using a standard fourth order Runge-Kutta routine with an ultimate step size of 0.005 cm tubule length. Reduction of the step size or the use of more sophisticated routines (Hamming's modified predictor-corrector method) did not alter the results to a significant degree. Execution time was of the order of 2.5 s. Inlet pressures were chosen to mimic measurements Schnermann made on loops microperfused at rates between 5 and 40 nl/min (32) (Fig. 2). Several runs were also carried out with an axial diffusion term, sign of $(dC_i/dx) D_i d^2C_i/dx^2$, included in the solute balances. The solution of the new equations led to difficulties due to the "stiffness" of the system. Rather than resort to extensive computation, we used a quick iterative approach to estimate the order of magnitude of the axial diffusion effect. The required second order derivative was calculated from concentration profiles obtained without axial diffusion, and the full equations solved repeatedly by this procedure. A small broadening of the profiles was observed at the tip of the loop and the lowest flow rates that were deemed not of sufficient importance for inclusion in the model.

Our first experiments used rat or rabbit parameters to model perfusion with 295 mosmol salt and 5 mosmol urea at 5–40 nl/min. By adjusting external salt and urea concentration profiles in the outer medulla we could produce curves relating water absorption and perfusion rate that resembled those found experimentally (25, 32, 35). However, external solute

concentrations required to achieve this result with rabbit parameters (Fig. 3) were much lower than measurements on kidney tissue slices would lead one to expect for rat kidneys (4, 27, 39). Medullary solute concentrations, used in conjunction with rat parameters, were much closer to those observed experimentally.

In these preliminary runs neither rat nor rabbit parameters correctly simulated urea transport by the rat loop. Micropuncture experiments indicate that in hydropenic rats twice as much urea leaves the loop as enters it (3). This was not the result produced by the models: with rabbit parameters urea was always absorbed, and less urea left the loop than entered it even when external urea concentration was 300 mM; with rat parameters too much urea was added to the loop. This was corrected by using K_u for DTL intermediate between those used in rat and rabbit (Table II).

As a further test of the model, the effects of perfusion with equilibrium solution were
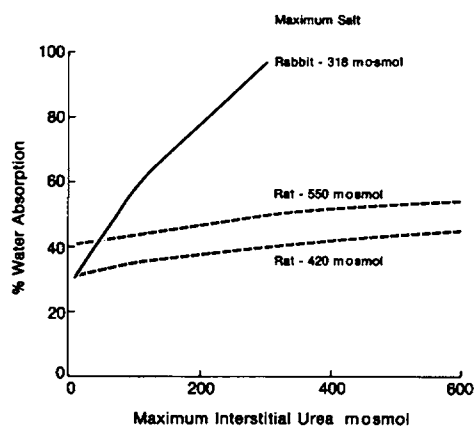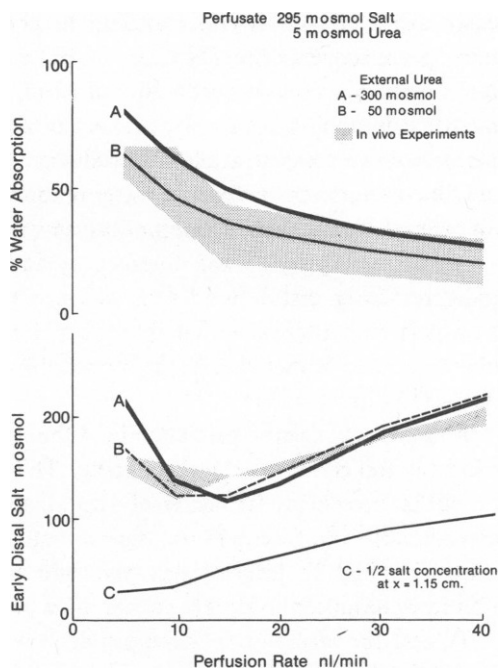
FIGURE 3

FIGURE 4

FIGURE 3   Percent water absorption with rat (dashed line) and rabbit (solid line) parameters in a model of Henle's loop. Perfusion rate (Q^0) constant at 15 nl/min. The exponent describing interstitial salt concentration in the "outer medulla" was set to give a maximum of 318 mosmol for rabbit and either 550 or 420 mosmol for rat. The exponent describing urea concentration in outer medulla was varied to demonstrate the relation between urea concentration and water reabsorption.

FIGURE 4   Comparison of in vivo saline microperfusion with computer simulations using the compromise model. The shaded area is bounded by data obtained from microperfusion experiments on rat superficial Henle's loops (25, 35). Lines represent output from the model with compromise parameters in either the rigid or compliant form with parameters constant and independent of radius. Curves A and C were obtained with a maximum external salt concentration in the medulla of 500 mosmol and a maximum urea concentration of 300 mosmol. Curve B maximum external urea, 50 mosmol/kg. Curve C, ½ salt concentration at $x = 1.15$ cm. This is equivalent to chloride concentration at the macula densa. For all the above runs $C_s^0 = 295$ mosmol, $C_u^0 = 5$ mosmol.

simulated. In these runs the perfusion fluid contained 80 mosmol raffinose and 220 mosmol salt with no urea. Reflection coefficient for raffinose was 1 and permeability was zero. There was no raffinose in the external medium. Under these conditions, models using rat or rabbit parameters did not reproduce the results of experiments in vivo (28). Instead of the 10–20% water absorption observed in microperfusion experiments, there was a net addition of water to the lumen. This defect was corrected by using parameters for PR obtained by Shafer et al. (30) and modifying DTL parameters by trial and error until the results of published microperfusion experiments with saline and equilibrium solutions were adequately reproduced. This procedure produced parameters that were roughly the average of rat and rabbit (Table II). Of course the values chosen were strongly influenced by the external salt and urea concentrations. If we had used lower maximum external solute concentration, the transport parameters would have resembled rabbit more than rat.

Models with only three segments, PR, DTL, and ATL, did not reproduce the relationship of early distal (ED) salt concentration to perfusion rate that has been observed in vivo. In microperfusion experiments (25, 35) ED salt concentration passes through a minimum at microperfusion rates between 10 and 15 nl/min. In attempts to reproduce this minimum we modified luminal pressure, V_m and K_m in ATL, and external solute concentration. At best a plateau of salt concentration was produced at perfusion rates between 5 and 10, but this could only be obtained by increasing water reabsorption to more than 95%. Curve C in Fig. 4 gives an example of the type of result obtained with a three-segment model.

A satisfactory result was obtained by adding a short ED segment. Experimental evidence indicates early distal tubules in rats are water impermeable with a much lower sodium transport rate than is found in proximal tubules (15). When an ED segment with these characteristics is included in the model effluent salt concentration is minimal at a 15 nl/min perfusion rate (Fig. 4).

In the model used to produce Fig. 4 the loop was rigid, that is to say, the lumen radius was constant and equal to (R_i), throughout. This model does not reproduce observed transit times or outlet pressures. Inclusion of the algebraic compliance relationships (Table I) led to considerable improvement in the fit between observed and simulated transit times and pressures (Fig. 2). Interestingly, the rigid and compliant models predicted the same absorption rates despite considerable differences in transit times.

To test the effect of radius-dependent permeabilities we compared the performance of a model in which permeation rates are independent of radius (Fig. 4) with models of compliant loops in which there is (a) 25% radius-dependent permeability in PR only, (b) complete radius-dependent permeability in each of the other segments taken singly, and (c) radius-dependent permeability in all the segments (Table III). The effects were small, amounting to at most a 4% increase in fractional water absorption and a 10% decrease in distal salt concentration. The model with radius-dependent permeabilities in all segments gave the best fit to experimental data. However, the difference from the output of the rigid model was small; therefore, we have used the simpler rigid form to construct all the figures except Fig. 2.

It should be noted that Fig. 4 et seq. were obtained using a rigid model with the same compromise parameters throughout. Outer medullary solute concentrations were set to resemble those in hydropenic rats (300 mosmol urea, 500 mosmol, [4, 39]; in Fig. 4 B they

TABLE III
EFFECT OF RADIUS-DEPENDENT PERMEABILITY ON FRACTIONAL WATER ABSORPTION AND DISTAL SALT CONCENTRATION

Perfusion rate	Rigid loop permeability constant	Compliant loop, permeability variable in one or all segments					Rigid loop permeability constant	Compliant loop, permeability variable in one or all segments				
							Distal sodium concentration	Change in distal sodium concentration				
		PR	DTL	ATL	ED	ALL*		PR	DTL	ATL	ED	ALL*
nl/min	% Water absorbed	Change in % water absorbed					mosmol	mosmol				
5	81.6	+1.4	+0.4	−0.1	+1.4	−1.2	216	+22	+18	+14	−7	−21
10	61.8	0	+0.3	−0.2	0	0	137	+8	+9	+3	0	−6
15	49.3	0	+0.9	−0.1	−0.1	+0.8	120	+4	+4	0	+1	−3
20	41.8	−1.7	+0.9	−1.0	−1.0	+0.6	135	+3	+2	+2	+2	0
30	31.5	−1.0	+0.5	−1.2	−1.2	+0.6	184	0	+1	0	0	0
40	25.3	−1.1	+0.4	−1.2	−1.2	+0.6	218	−1	+1	−1	−1	+1

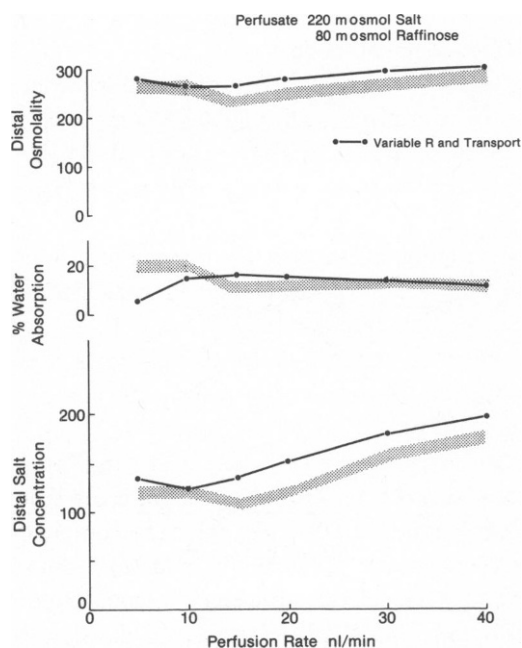*This form gives the best fit to experimental data (Fig. 4).

FIGURE 5
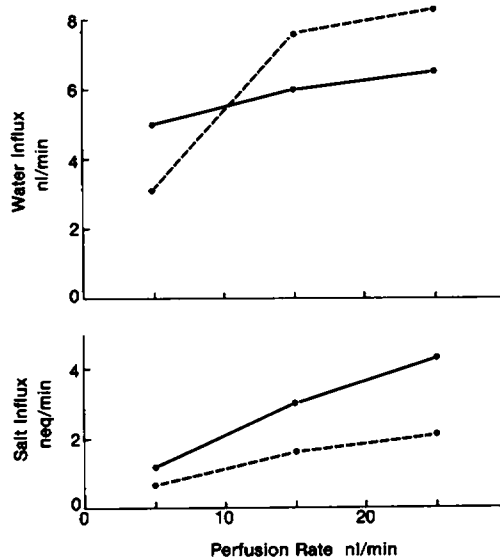
FIGURE 6

FIGURE 5   Comparison of in vivo "equilibrium" solution microperfusions with computer simulations. The shaded area represents the mean ± SEM for the data obtained in microperfusion experiments (25). Lines were produced by the model with compromise parameters, 220 mosmol, C^0_{Ra} − 80 mosmol, C^0_s − 0.

FIGURE 6   Salt concentration in and percent water absorption from loops perfused with 300 mM mannitol. Results of computer simulations are shown in solid lines and results of in vivo microperfusion are shown as dashed lines (35).

were also set to resemble saline diuretic rats (50 mosmol urea, 500 mosmol salt, [39]). The model incorporating compromise parameters simulates results obtained with so-called equilibrium solution (Fig. 5) and the relationship between perfusion rate and water flux in a loop perfused with 300 mosmol mannitol (35) (Fig. 6). It also mimics the effects of inhibiting active transport in the loop. Fig. 7 compares the effects of removing active transport from PR and ATL of the model with results obtained using four inhibitors of salt transport in the microperfused rat loops (41). The agreement is best between model and triflocin or furosemide inhibition. Both of these compounds probably inhibit active transport in ATL and PR (37).

DISCUSSION

Choice of Model and Model Parameters

One of our objectives in modeling Henle's loop was to integrate measurements of tubule wall parameters obtained in vitro from isolated fragments with in vivo measurements of overall function of a single microperfused loop. There are wide ranges in the values found experimentally for some tubule parameters. Those used in preliminary models labeled rabbit
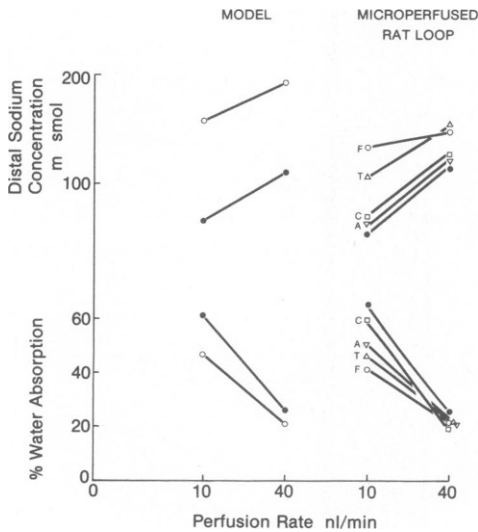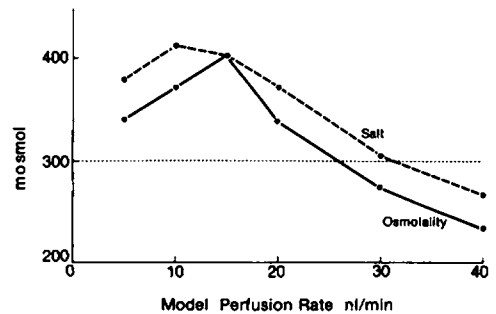

FIGURE 7

FIGURE 8

FIGURE 7 Model compared with microperfusion experiments (41). The solid circles on the model indicate output from the model including active transport. Solid circles on the microperfusion experiments indicate in vivo microperfusion with Ringer's solution. Open circles on the left indicate results obtained when active transport is removed from the model. The open symbols on the right show results obtained by Wright et al. (41) when they microperfused Ringer's solution including one of four inhibitors. A, amiloride, C, cyanide, F, furosemide, T, triflocin.

FIGURE 8 Mean concentration of fluid absorbed in the outer medulla which begins at $x = 0.4$ cm and ends at $x = 0.9$ cm. Mean salt concentration was calculated as follows: $[C_{s,0.4} - (Q_{0.9}/Q_{0.4})C_s0.9]/[1 - Q_{0.9}/Q_{0.4}]$. Total salt plus urea concentration was inserted into this equation to calculate osmolality of reabsorbed fluid.

and rat represent the extremes of available measurements. The parameters used in rat gave the DTL low water and high solute permeabilities, whereas the converse was true for rabbit where water permeability was 4 times greater, urea premeability $\frac{1}{10}$ and salt permeability $\frac{1}{30}$ that for rat. Rabbit and rat also represent two types of concentrating systems that have been proposed to explain medullary counter-current function (19): water extraction is the primary concentrating process in rabbit DTL, and combined solute addition and water extraction operates in rat.

Rabbit loops have not been microperfused in vivo; therefore, because there is no way to check the validity of computer simulations, we did not set out to model the rabbit loop. Nonetheless, our results show that rat loops with permeabilities like those of rabbit would not add urea to the loop and must function with low medullary interstitial urea concentrations. This prediction agrees with the free flow micropuncture experiments of Roch-Ramel et al. (28) who found that no urea is added to superficial Henle's loops in rabbits and the papillary urea concentration in dehydrated rabbits is one quarter that found in dehydrated rats. In contrast, when rat parameters are used, urea is added to the loop and water absorption is similar to that observed in microperfused rat loops (Fig. 3) (25, 32). Note, our simulation does not deal with the mechanism responsible for accumulation of urea in the medullary interstitium, but it does indicate how tubule parameters and interstitial urea concentration interact in a single microperfused loop.

Modifications were necessary before the model correctly predicted the results of perfusion with equilibrium solution. This was done by altering transport parameters in the PR and choosing a compromise between rat and rabbit parameters to describe the DTL (Table II). In the model using compromise parameters external salt and urea concentrations were set to reproduce the composition of tissue from hydropenic rats. Salt concentration rose from 295 to 500 mosmol; urea rose from 5 to 300 mosmol (Fig. 1). The exponential shape of these gradients over 2.5 mm is consistent with electron-probe measurements of tissue slices (22), with chemical analysis of mulitple tissue slices (4) and with gradients generated by other mathematical models of the medulla (10, 11).

Water Absorption

Removing active transport from the model decreases water absorption 10–15%. This is almost exactly the effect observed when salt transport is inhibited in vivo by microperfusing the loop with furosemide (41) (Fig. 8). In the model the residual water absorption is driven primarily by osmotic pressure differences across the DTL. It is reasonable to assume that the same forces operate in vivo.

If water absorption from the loop is, in fact, driven osmotically by the external solute concentration in the outer medulla we should see relationships between loop water absorption and medullary solute concentration.

Schnermann (32) did observe less water absorption from microperfused loops of saline diuretic rats than than from loops of dehydrated rats. Urea concentration in the outer medulla decreases with saline diuresis, but salt concentration rises slightly and osmolality is unchanged (4). We simulated this condition by reducing maximum external urea concentration to 50 mosmol. This modification of the outer medullary interstitium produced decreases in water absorption (Fig. 4, curve B) similar to those resulting from saline-diuresis in vivo (32).

With respect to water absorption there appears to be a contradiction between the model's predictions and in vivo experiments on water diuretic animals. Water diuresis is associated with decreased salt and urea concentrations in the outer medulla (4, 27, 39). Under these conditions our model predicts decreased water absorption by the loop; however, in several free-flow micropuncture studies, loop water absorption was either unchanged or increased during water diuresis (2, 19, 34). The model could account for these experimental observations if either surface area or permeability in DTL were altered by the water diuresis. The increase in transit time observed in some micropuncture experiments suggests an increase in luminal volume and wall surface area (34). Evidence exists that a large decrease in medullary urea concentration, which accompanies the water diuresis, could alter tubule wall permeability (12). Also possible are hormone-induced changes in wall permeability.

Effect of Tubular Diameter

Most models of Henle's loop assume a rigid tube or one in which permeabilities are constant (10, 11, 17, 38). By incorporating compliance in our model we obtained an improved simulation of transit times and distal pressures (Fig. 2).

Although transit times, especially at low perfusion rates, differ greatly in the rigid and compliant models, there is no difference in the absorption of solutes or water (Fig. 4 represents both forms of the model). In other words, according to the assumptions used in formulating these models transit time (or contact time) has no effect on absorption.

An apparent relationship between transit time and absorption could appear if wall permeability depends on luminal radius and/or wall thickness. Burg and Orloff (7) found a significant 19% increase in water efflux when the diameter of isolated proximal tubules was increased from 15 to 26 μm. It appears likely that most of the resistance to transcellular flux of solute resides in the tight junction of proximal tubules (30, 31). Permeability of the tight junction is probably independent of luminal diameter. But the resistance offered by intercellular channels may well be the site of the diameter-dependent permeability change that Burg and Orloff observed. In accordance with this conception of proximal tubular function, we made 25% of the PR permeability dependent on luminal diameter (Table III).

In the distal tubule an increase of luminal pressure produces dramatic decreases in the transcellular potential difference (13). This phenomenon may result from altered active transport or from an increase in passive salt back flux when lumen diameter dilates in response to increased pressure.

To our knowledge there is no experimental study of radius permeability relationships in the DTL. One may speculate that because of deep tight junctions in the DTL (33) water flux occurs primarily across the cell walls. In this case permeation rate may be a function of luminal surface area and cell thickness. The luminal surface of DTL cells is free of microvilli, hence the surface area will change as the lumen dilates or contracts. It is of course possible that solute and water permeabilities are affected to different extents by changes in diameter.

Including radius-dependent permeabilities in a loop with algebraic compliance produces small changes in solute and water absorption (Table III). The results obtained by perfusing a rat loop at 5–40 nl/min can be simulated almost as well by a loop with constant wall parameters that are independent of radius.

Salt Concentration in Early Distal Tubule

A puzzling feature of loop microperfusion studies is the minimum salt concentration found in ED at perfusion rates between 10 and 15 nl/min. This minimum in the curve relating ED salt concentration and perfusion rate was not reproducible with a three segment model, but was produced by addition of a short ED segment (Fig. 4). Schnermann et al. (35) suggested that salt concentration rises due to osmotically driven water absorption in the ED when flow is slow. In our model the addition of a water permeable ED would lead to unacceptably high water absorption at 5–10 nl/min perfusion rates; therefore we added a water-impermeable tubule with an active transport rate considerably lower than that in the ATL. The characteristics of this ED segment are consistent with available experimental data (15). With this segment added, distal salt concentration rose due to increased influx of salt.

With the compromise parameters, chloride (salt $\times$ 0.5) concentration at the macula densa ($x = 1.15$ cm) was 30–35 mosmol for perfusion rates of 5–10 nl/min (Fig. 4). At higher perfusion rates the concentration at the macula densa was a monotonic function of perfusion rate. At low flow rates chloride concentration was close to the value of 25 mM Schnermann et al. (36) deduced from the results of retrograde microperfusion experiments.

TABLE IV

SIGNIFICANCE OF ASSUMPTIONS USED IN THE COMPUTER MODEL

Assumption	Result
Rabbit parameters	Defects: (*a*) water absorption very sensitive to external salt and urea (Fig. 3); (*b*) water added to loop perfused with equilibrium solution; (*c*) urea not recirculated.
Rat parameters	Defects: (*a*) too much urea recirculated; (*b*) water added to loop perfused with equilibrium solution.
Compromise	Advantages: (*a*) correctly predicts absorption when equilibrium solution is perfused (Fig. 5); (*b*) improved prediction of response to changes in external urea (cf. A and B, Fig. 4); (*c*) improved prediction of urea recirculation; (*d*) predicts response to perfusion with 300 mosmol mannitol (Fig. 6) and inhibitors of active transport (Fig. 7).
Active salt transport in ED < ATL	Advantage: predicts minimum salt concentration in effluent at perfusion rate of 15 nl/min (Fig. 4).
Rigid tube	Defects: (*a*) reabsorption too high at perfusion rates below 30 nl/min (Fig. 4); (*b*) transit times differ from those observed; (*c*) distal pressures differ from those observed.
Compliant loop with constant permeability	Advantages: improved prediction of transit times and distal pressures. Defects: (*a*) does not alter predicted reabsorption (Fig. 4); (*b*) does not predict observation relationships among absorption, transit time, and distal tubule pressure (5).
Compliant loop with radius-dependent transport in all segments	Advantages: (*a*) fractional water absorption decreases at low perfusion rates and increases at high perfusion rates; (*b*) improved fit of effluent salt concentration to observed results. Defect: effects are too small to be tested experimentally by varying microperfusion rate.

Counter-Current Multiplication by the Model Loop

Let us now examine whether or not the model with compromise parameters could function in a counter-current multiplication system. To provide the single effect that is multiplied, the loop must add solute to the outer medullary interstitium. This implies that, in the medulla, solute concentration in the reabsorbate is greater than concentration in the cortical interstitium. The mean concentration of salt in fluid leaving the loop between $x = 0.4$ and $x = 0.9$ cm exceeded that in the cortical interstitium for flows between 5 and 30 nl/min (Fig. 8). The peak salt concentration in the reabsorbate occurred at a perfusion rate of 10 nl/min, whereas the peak osmolality was obtained at 15 nl/min; therefore, the loop would contribute most effectively to a counter-current system at flow rates in the physiological range.

In summary, simple phenomenological transport equations combined with in vitro measurements of tubule characteristics were used to create a mathematical model of a rat short Henle's loop. The model simulates loop function at perfusion rates between 5 and 40 nl/min when the perfusion solution is either saline or equilibrium solution or 300 mM mannitol or saline plus furosemide. Addition of urea to the loop resembles that found experimentally. Water absorption is largely driven by osmotic forces operating across the DTL. Salt concentration at the macula densa is a monotonic increasing function of perfusion rate; the concentration at perfusion rates of 5–10 nl/min is in the range deduced from microperfusion experiments. Salt concentration at the end of the model loop passes through a minimum at a perfusion rate of 15 nl/min. This is similar to the behavior of loops microperfused in vivo. The assumptions used in creating this model and their consequences are summarized in Table IV.

REFERENCES

1. ANAGNOSTOPOULOS, T., M. J. KINNEY, and E. E. WINDHAGER. 1971. Salt and water reabsorption by short loops of Henle during renal vein constriction. *Am. J. Physiol.* 220:1060–1066.
2. ANTONIOU, L. D., T. J. BURKE, R. R. ROBINSON, and J. R. CLAPP. 1973. Vasopressin related alterations of sodium reabsorption in the loop of Henle. *Kidney Int.* 3:6–13.
3. ARMSEN, T., and H. W. REINHARDT. 1971. Transtubular movement of urea at different degrees of water diuresis. *Pfluegers Arch. Eur. J. Physiol.* 326:270–280.
4. ATHERTON, J. C., R. GREEN, and S. THOMAS. 1970. Effects of 0.9% saline infusion on urinary and renal tissue composition in the hydropenic normal and hydrated conscious rat. *J. Physiol.* 210:45–71.
5. BAINES, A. D. 1975. The effect of lowering and raising distal tubular pressure on reabsorption from microperfused loops of Henle. *Proc. 6th Int. Congr. Nephrol.* 182. (Abstr.)
6. BASMADJIAN, D., and A. D. BAINES. 1978. Examination of transport equations pertaining to permeable elastic tubules such as Henle's loop. *Biophys. J.* 24:629–643.
7. BURG, M. B., and J. ORLOFF. 1973. Perfusion of isolated renal tubules. *Handb. Physiol.* (Renal Physiology) 8:145–159.
8. CORTELL, S., F. J. GENNARI, M. DAVIDMAN, W. H. BOSSERT, and W. B. SCHWARTZ. 1973. Definition of proximal and tubular compliance. Practical and theoretical implications. *J. Clin. Invest.* 52:2330–2339.
9. CURRAN, P. F., and S. G. SCHULTZ. 1976. Some thermodynamic and kinetic principles governing solvent and solute transport across membranes. *In* The Kidney. B. M. Brenner and F. C. Rector, Jr., editors. W. B. Saunders Co., Philadelphia. 104–125.

10. FOSTER, D., J. A. JACQUEZ, and E. DANIELS. 1976. Solute concentration in the kidney II. Input-output studies on a central core model. *Math. Biosci.* **32**:337–360.

11. FOSTER, D. M., and J. A. JACQUEZ. 1978. Comparison using central core model of renal medulla of the rabbit and rat. *Am. J. Physiol.* **234**:F402–F414.

12. FOWLER, N., E. GONZALEZ, F. A. RAWLINS, G. H. GIEBISCH, and G. WHITTEMBURY. 1977. Effect of hypertonic urea and mannitol on distal nephron permeability. *Pfluegers Arch. Eur. J. Physiol.* **368**:3–11.

13. GROSS, J. B., M. IMAI, and J. P. KOKKO. 1975. A functional comparison of the cortical collecting tubule and the distal convoluted tubule. *J. Clin. Invest.* **55**:1284–1294.

14. HEBERT, L. A., and G. S. ARBUS. 1971. Renal subcapsular pressure—a new intrarenal pressure measurement. *Am. J. Physiol.* **220**:1129–1136.

15. HIERHOLZER, K., and M. WIEDERHOLT. 1976. Some aspects of distal tubular solute and water transport. *Kidney Int.* **9**:198–213.

16. IMAI, M. 1977. Function of the thin ascending limb of Henle of rats and hamsters perfused in vitro. *Am. J. Physiol.* **232**:F201–F209.

17. JACQUEZ, J. A., D. FOSTER, and E. DANIELS. 1976. Solute concentration in the kidney. 1. A model of the renal medulla and its limit cases. *Math. Biosci.* **32**:307–335.

18. JAMISON, R. L. 1974. Counter-current systems. *In MTP International Rev. Sci.* **6**: Kidney and urinary tract physiology. K. Thurau, editor. Butterworths, London. 199–245.

19. JOHNSTON, P. A., F. B. LACY, and R. L. JAMISON. 1977. Effect of antidiuretic hormone-induced antidiuresis on water reabsorption by the superficial loop of Henle in Brattle bozo rats. *J. Lab. Clin. Med.* **90**:1004–1011.

20. KALLSKOG, O., L. O. LINDBOM, H. R. ULFENDAHL, and M. WOLGAST. 1976. Hydrostatic pressures within the vascular structures of the rat kidney. *Pfluegers Arch. Evr. J. Physiol.* **363**:205–210.

21. KNOX, F. G., L. R. WILLIS, J. W. STRANDHOY, E. G. SCHNEIDER, L. G. NAVAR, and C. E. OTT. 1972. Role of peritubular Starling forces in proximal reabsorption following albumin infusion. *Am. J. Physiol.* **223**:741–749.

22. KOEPSELL, H., W. A. P. NICHOLSON, W. KRIZ, and H. J. HÖHLING. 1974. Measurements of exponential gradients of sodium and chloride in the rat kidney medulla using the electron microprobe. *Pfluegers Arch. Eur. J. Physiol.* **350**:167–184.

23. KOH, Y. G., and A. D. BAINES. 1974. Pressure flow relationships in Henle's loops and long collapsible rubber tubes. *Kidney Int.* **5**:30–38.

24. KREITH, F. 1973. Principles of Heat Transfer. 3rd edition. International Text Book Co., Scranton, Pa. 30.

25. MORGAN, T., and R. W. BERLINER. 1969. A study by continuous microperfusion of water and electrolyte movements in the loop of Henle and distal tubule of the rat. *Nephron.* **6**:388–405.

26. MUNKÁCSI, I., and M. PALKOVITS. 1966. Study on the renal pyramid, loops of Henle and percentage distribution of their thin segments in mammals living in desert, semi-desert and water-rich environment. *Acta Biol. Acad. Sci. Hung.* **17**:89–104.

27. PERLMUTT, J. H. 1962. Influence of hydration on renal function and medullary sodium during vasopressin infusion. *Am. J. Physiol.* **202**:1098–1104.

28. ROCH-RAMEL, F., B. FILLOUX, J. P. GUIGNARD, and G. PETERS. 1978. Fate of urea in Henle's loops of the rabbit and rat. Proceedings of the 6th Workshop Conference Hoechst. Excerpta Medica., Amsterdam. 118–121.

29. SANJANA, V. M., P. A. JOHNSTON, W. M. DEEN, C. R. ROBERTSON, B. M. BRENNER, and R. L. JAMISON. 1975. Hydraulic and oncotic pressure measurements in inner medulla of mammalian kidney. *Am. J. Physiol.* **228**:1921–1926.

30. SCHAFER, J. A., C. S. PATLADE, S. L. TROUTMAN, and T. E. ANDREOLI. 1978. Volume absorption in the pars recta, II Hydraulic conductivity coefficient. *Am. J. Physiol.* **234**:F340–F348.

31. SCHAFER, J. A., C. S. PATLUK, and T. E. ANDREOLI. 1977. Fluid absorption and active and passive ion flows in the rabbit superficial pars recta. *Am. J. Physiol.* **233**:F154–F167.

32. SCHNERMANN, J. 1968. Microperfusion of single short loops of Henle in rat kidney. *Pfluegers Archiv. Gesamte Physiol. Menschen Tiere.* **300**:255–282.

33. SCHNERMANN, J., D. W. PLOTH, and M. HERMLE. 1976. Activation of tubulo-glomerular feedback by chloride transport. *Pfluegers Arch. Eur. J. Physiol.* **362**:229–240.

34. SCHNERMANN, J., H. VALTIN, K. THURAU, W. NAGEL, M. HORSTER, H. FISCHBACH, M. WAHL, and G. LIEBAU. 1969. Micropuncture studies on the influence of antidiuretic hormone on tubular fluid reabsorption in rats with hereditary hypothalamic diabetes insipidus. *Pfluegers Archiv. Gesamte Physiol. Menschen Tiere.* **306**:103–118.

35. SCHNERMANN, J., F. S. WRIGHT, J. M. DAVIS, W. V. STACKELBERG, and G. GRILL. 1970. Regulation of superficial nephron filtration rate by tubulo-glomerular feedback. *Pfluegers Arch. Eur. J. Physiol.* **318**:147–175.

36. SCHWARTZ M. M., and M. A. VENKATACHALAM. 1974. Structural differences in thin limbs of Henle: physiological implications. *Kidney Int.* 4:193–208.
37. SEELY, J. F., and J. H. DIRKS. 1977. Site of action of diuretic drugs. *Kidney Int.* 11:1–8.
38. STEPHENSON, J. L., R. MEJIA, and R. P. TEWARSON. 1976. Model of solute and water movement in the kidney. *Proc. Natl. Acad. Sci. U.S.A.* 73:252–256.
39. VALTIN, H. 1966. Sequestration of urea and non-urea solutes in renal tissues of rats with hereditary hypothalamic diabetes insipidus. Effect of vasopressin and dehydration on the counter-current mechanism. *J. Clin. Invest.* 45:337–334.
40. WELLING, L. W. and D. J. WELLING. 1978. Physical properties of isolated perfused membranes from rabbit loop of Henle. *Am. J. Physiol.* 234:F54–F58.
41. WRIGHT, F. S., and J. SCHNERMANN. 1974. Interference with feedback control of glomerular filtration rate by furosemide, triflocin and cyanide. *J. Clin. Invest.* 53:1695–1708.